Heliyon 10 (2024) e36016

Contents lists available at ScienceDirect

Heliyon

journal homepage: www.cell.com/heliyon

Research article

The combination of apatinib and antigen-specific DC-induced T cells exert antitumor effects by potently improving the immune microenvironment of osteosarcoma

Tu Hu [a,b,1], Wei Sun [a,b,1], Yongjia Jin [c,1], Yan Dong [c], Wanlin Liu [c], Zhengwang Sun [a,b], Yang Xiang [c,**], Yong Chen [a,b,d,*]

[a] Department of Musculoskeletal Surgery, Fudan University Shanghai Cancer Center, Shanghai, China
[b] Department of Oncology, Shanghai Medical College, Fudan University, Shanghai, China
[c] Shanghai Electric Power Hospital, Shanghai, China
[d] Minhang Branch of Fudan University Shanghai Cancer Center, Shanghai, China

ARTICLE INFO

Keywords:
Osteosarcoma
Apatinib
DC-T
MDSC
TAM
Immunity

ABSTRACT

Objective: Osteosarcoma (OS) is the most common primary bone sarcoma with a high propensity for local invasion and metastasis. Although the antitumor effect of apatinib has been well confirmed in advanced OS, the synergistic effect of apatinib and immunotherapies has not yet been elucidated.

Methods: In this study, we established tumour-bearing mice and observed tumour size with low and high doses of apatinib treatments. The expression of 17 cytokines, including vascular endothelial growth factor (VEGF), was detected by protein microarray analysis. Moreover, we designed apatinib and antigen-specific dendritic cell (DC)-T combination treatment for tumour-bearing mice. Tumour growth was detected by statistical analysis of tumour size and microvessel density (MVD) counting, the protein expression of VEGF by western blotting, the cytokines interleukin 6 (IL-6), IL-17 and interferon-gamma (IFN-γ) by enzyme-linked immunosorbent assay (ELISA), and the numbers of myeloid-derived suppressor cells (MDSCs) and tumour-infiltration macrophages (TAMs) by flow cytometry.

Results: The results showed that apatinib efficiently suppressed tumour growth, and high-dose apatinib achieved a stronger effect. The same was true for DC-T immunotherapy. However, their combination treatment revealed a better oncolytic effect. Meanwhile, apatinib or DC-T treatment inhibited the expression of VEGF and the proangiogenic mediators IL-6 and IL-17 but increased IFN-γ production. Combination therapy further reduced/increased these effects. In addition, the combination treatment reduced MDSC but enhanced TAM-M1 ratios in the OS microenvironment. These findings indicated that apatinib and antigen-specific DC-T combination therapy was more efficient in oncolysis by regulating pro-/anti-angiogenic inducers and improving the immune state in the OS microenvironment.

Conclusion: This study proved that it was feasible to employ immunotherapy with therapeutic agents in OS treatment, which may provide a new approach in addition to the combination of surgery with chemotherapy in tumour treatment.

* Corresponding author. No. 270, DongAn Road, Shanghai, China.
** Corresponding author. No. 937, Yananxi Road, Changning District, Shanghai, China.
E-mail addresses: dlyy1951@163.com (Y. Xiang), chenyong@fudan.edu.cn (Y. Chen).
[1] Contributed equally to this work.

https://doi.org/10.1016/j.heliyon.2024.e36016
Received 13 June 2023; Received in revised form 4 July 2024; Accepted 7 August 2024
Available online 8 August 2024
2405-8440/© 2024 Published by Elsevier Ltd. This is an open access article under the CC BY-NC-ND license (http://creativecommons.org/licenses/by-nc-nd/4.0/).

1. Introduction

OS is the most common primary malignant bone tumour that commonly occurs in children and adolescents with very low patient survival [1]. The worldwide OS incidence is approximately one to three million annually [2]. With the development of current therapeutic management, the 5-year survival rate has increased from less than 20 % to the current 50–70 %, but many patients still die of recurrence and metastasis [3]. Data from China showed that approximately 12.6 % of OS patients have developed distant metastases when receiving treatment, approximately 9 % of patients have local recurrence within 36 months after treatment, and more than 30 % of patients still develop distant organ metastasis after treatment [4,5]. In addition, the systemic toxicity side effects caused by high doses of chemotherapeutic drugs, as well as drug resistance due to the heterogeneity of osteosarcoma, restrict the curative effect of chemotherapeutic drugs and ultimately lead to low OS clinical efficacy [6].

As a new treatment method, immunotherapy can effectively control some tumours, even those large ones that are out of control by chemotherapy/radiotherapy [7]. Therefore, immunotherapy has attracted increasing attention in the global medical field. Recently, studies have revealed that immune cells such as MDSCs, TAMs, immature dendritic cells (imDCs), and proinflammatory cytokines such as IL-6, IL-17, and TNF-α promote tumour progression by stimulating angiogenesis and tissue remodelling and form an inhibitory immune state in the OS microenvironment [8–10], which is able to convert killer T cells to suppressor Tregs and leads to low clinical efficacy of immunotherapy [11,12]. Tumour-educated MSCs (TEMSC) was found to boost osteosarcoma growth and pulmonary metastasis. However, this cancer-promoting effects could be abolished by coadministration of a therapeutic IL6 receptor (IL6R) antibody [13]. Moreover, a whole transcriptome analysis from osteosarcoma patients revealed ectopic expressions of butyrophilin-like 9 (BTNL9) and transforming growth factor-beta-induced gene (TGFBI), two crucial genes regulating immune homeostasis in various cancers [14]. BTNL9 was involved in modulating the T cell response and impacting inflammatory disorders and cancers [15]. And TGFBI plays a crucial role in tumour cell proliferation, angiogenesis, and apoptosis, demonstrated immunosuppressive effects within the tumour immune microenvironment [16]. Whole exome sequencing of osteosarcoma and normal bone and their expression of repetitive DNA elements (they regulate innate immunity) were also been analysed [17,18]. The researchers found the WNT/β-catenin signalling pathway and the IGF1/IGF2 and IGF1R homodimer signalling and TP53 pathways might have a role in osteosarcoma development.

Angiogenesis, characterized by disorganized and permeable blood vessels, is a fundamental biological feature of tumours, during which tumour cells release a series of proangiogenic factors [19,20]. Recent evidence indicates that vascular endothelial growth factor (VEGF) is a major contributor to tumour angiogenesis, promoting tumour development [21–23]. VEGF is a homodimeric glycoprotein recognized by VEGF receptors (VEGFRs) that are predominantly expressed in vascular endothelial cells [24]. The production of VEGF makes new blood vessels form in and around tumour tissues by increasing oncogene expression, which results in exponential tumour growth [24]. Therefore, inhibition of angiogenesis by blocking VEGF and the corresponding VEGFR activities has been validated to be efficient for cancer therapeutic management [25,26]. In preclinical studies, antiangiogenic drugs targeting VEGF have synergistic effects with immunotherapy. A recent study demonstrated that the normalization of tumour vascular structure caused by anti-VEGF antibody increased the infiltration of transfused adoptive T cells in the tumour and significantly improved the efficiency of adoptive cell infusion-based immunotherapy in tumour-bearing animals [27]. Apatinib, as an inhibitor of VEGFR, is considered to be an efficient VEGF-TKI in anti-angiogenesis with mild toxicity and drug resistance. Although analysis of human gene regulation reveals that VEGF-TKIs downregulate angiogenic signalling pathways in microvascular endothelial cells and the antitumor effect of apatinib has been well confirmed in human advanced OS, the synergistic effect between apatinib and antigen-specific DC-T immunotherapy has not yet been elucidated, and the mechanisms underlying the antitumor effect of the combination therapy are still unclear.

Inflammation is closely associated with cancer initiation and progression [28]. Inflammatory mediators are closely related to proangiogenic factors in the tumour microenvironment. The potent proinflammatory inducers IL-6 and IL-17 exert proangiogenic effects in the tumour microenvironments of various solid tumours [29–31]. IFN-γ is thought to be an anti-angiogenic cytokine [32]. Thus, in this study, we established Lewis tumour-bearing mice and treated them with different doses of apatinib. Moreover, we performed apatinib and OS antigen-specific DC-T combination treatment in OS mice. After detecting tumour growth, the protein levels of VEGF and key cytokines, and the numbers of MDSC and TAM immune cells with different treatments in the OS microenvironment, we demonstrated that the combination of apatinib and DC-T immunotherapy was more efficient in antitumor angiogenesis and immune microenvironment improvement to inhibit tumour growth. Thus, this study provides strong evidence for the exploration of employing immunotherapy with therapeutic agents in OS treatment.

2. Materials and methods

2.1. Animal experiment

Male G57BL/6 mice (6 weeks old, 18–22 g) were purchased from Beijing Laboratory Animal Center, Chinese Academy of Sciences, and were inoculated with HOS-8603 human osteosarcoma cells (s.c. 2×10^5 cells/mouse) to establish tumour-bearing mice. Eight days later, all tumour-bearing mice were randomly divided into three groups, and each group contained 8 mice. Two groups were given 50 mg/kg/d and 200 mg/kg/d apatinib (i.t.) interventions every day, with mice given an equal volume of PBS solution (i.t.) as a control. We observed tumour growth and measured tumour diameter every other day. After 18 consecutive days of dosing, all mice were sacrificed, and tumour tissues were isolated from the mice for the following experiment.

2.2. Measurement of tumour volume

The maximum long and short diameters of the tumours in tumour-bearing mice were measured with Vernier callipers every other day, and the average tumour volume of each group was calculated. Tumour volume = tumour long diameter × tumour short diameter $^2/2$.

2.3. Protein microarray

The obtained tumour tissues were cut into small pieces, and the lysates were added on ice for 20 min. A tissue homogenizer was used to break the tissue, which was centrifuged at 14,000 rpm for 20 min. Then, the tumour tissues were transferred to 2 mL centrifuge tubes for protein microarray. The 17 pro/anti-angiogenic factors were detected according to the instructions of the human cytokine antibody array (Raybiotech, USA). Microarry Suite 5.0 and Significance Analysis of Microarray (SAM) software were applied to analyse the results. Ratios >1.5 or <0.67 were considered different in cluster analysis.

2.4. Freeze–thawed antigen preparation of HOS-8603 cells

HOS-8603 cells were resuspended in 0.5 mL Roswell Park Memorial Institute (RPMI)-1640 medium (Sigma, US) after washing with PBS twice and pipetting to mix. After that, the mixtures were frozen and thawed at −80 °C and 42 °C 3 times to lyse the cells, centrifuged at 15,000 rpm for 30 min, and the supernatant was collected. Finally, the collected supernatant was sterilized by filtration and kept at 4 °C.

2.5. Mouse spleen T lymphocyte culture

The C57BL/6 mice were killed by cervical dislocation and soaked in 75 % ethanol for 2 min. Then, the spleen was isolated under sterile conditions and washed with PBS. The isolated spleen was ground with a sterile glass grinding rod, filtered through a 200-mesh aluminium stainless steel mesh, and rinsed with PBS. The spleen cells were then collected in a centrifuge tube and centrifuged at 2000 rpm for 5 min. The supernatant was discarded, and the cells were resuspended in PBS and pipetted until mixed. After that, the spleen cell suspension was carefully added to the upper layer of mouse lymphocyte separation medium at a ratio of 2:1 in a new centrifuge tube under sterile conditions and centrifuged at 1800 rpm for 20 min. The buffy coat of the upper and middle layers was carefully aspirated and placed in another centrifuge tube. Then, RPMI-1640 medium was added, mixed with a pipette, and centrifuged at 2000 rpm. The supernatant was discarded, and the washing was repeated twice. Finally, 5 mL RPMI-1640 medium was added to the collected cells and mixed with a pipette. The cells were counted, and their activity was detected for the following experiment.

2.6. Mouse bone marrow-derived tumour antigen-specific DC culture

The C57BL/6 mice were killed by cervical dislocation and soaked in 75 % ethanol for 2 min. The femur and tibia were removed under sterile conditions, rinsed with PBS, and then soaked in 75 % ethanol for 2 min. The bone marrow cavity was rinsed with RPMI-1640 medium, the bone marrow was collected in a Petri dish with a 200-mesh cell screen in advance, and the bone marrow cavity was repeatedly washed 4–6 times. The bone marrow suspension was ground and collected in a Petri dish, transferred to a centrifuge tube, centrifuged at 12,000 rpm for 5 min, and resuspended in PBS. Mouse lymphocyte separation medium was used to separate and obtain DCs according to the same method as described above to isolate mouse spleen T cells. After 6 days of in vitro culture, the DCs were mixed with the freeze–thawed antigen from the HOS-8603 cells at a ratio of 1:5, supplied with 20 ng/mL rMTNF-a, and incubated under 5 % CO2 at 37 °C. Cell colonies were observed daily during induction, and the growth of DCs was recorded.

2.7. Co-culture of DC-T cells

Nine days after the DCs were induced with tumour antigens, the mature DCs were collected, and the cell concentration was adjusted to 1×10^6/mL. Mitomycin (2.5 μg/mL) was added, and the cells were incubated at 37 °C for 30 min. Then, the cells were washed with RPMI-1640 medium 3 times, and the cell concentration was readjusted to 1×10^6/mL. Then, the tumour antigen-specific DCs and spleen T cells were mixed at a ratio of 1:10 and incubated for 24 h. The tumour antigen-specific DC-T cells were prepared.

2.8. Efficacy evaluation of apatinib combined with DC-T cells in an OS mouse model

The tumour-bearing mice were established as above and randomly divided into 4 groups, named the PBS group, DC-T group, apatinib group and apatinib + DC-T group, and each group contained 8 mice. Seven days after Lewis tumour-bearing mice were established, the apatinib group mice were injected with apatinib 15 mg/kg/d (i.t.); the DC-T group mice were injected with 1×10^6 tumour antigen-specific DC-T cells (i.t.); the apatinib + DC-T group mice were injected with apatinib 15 mg/kg/d and injected one week later with 1×10^6 tumour antigen-specific DC-T cells (i.t.); and the PBS group mice were injected with an equal volume of PBS solution (i.t.). Tumour growth was observed every day; 14 days later, all the mice were sacrificed, and the tumour tissues were aseptically isolated for subsequent experiments.

2.9. MVD detection

The tumour tissues were fixed in paraformaldehyde, embedded in paraffin, dewaxed and rehydrated. The streptavidin-peroxidase (SP) method was applied to detect the MVD levels with different treatments in OS mice. The average number of blood vessels was observed and counted under a microscope. Five high-magnification fields (200 ×) were counted for each slice, and the average number in one view was presented as the MVD.

2.10. Flow cytometry analysis

The tumour tissues were separated and cut into small pieces, digested with trypsin, filtered through a 300-mesh filter to obtain a single-cell suspension, and adjusted to a cell concentration of 5×10^5/mL. Then, 100 μL of cell suspension was added to each flow tube, and PE-conjugated Gr-1 antibody, FITC-conjugated CD11b antibody, APC-conjugated iNOS antibody, FITC-conjugated CD206 antibody, PE-conjugated CD68 antibody and FITC-conjugated CD206 antibody were added. The cell suspensions and the fluorescently labelled antibodies were mixed and kept at room temperature for 30 min in the dark. Flow cytometry (FACS Aria II, Becton, Dickinson and Company) and Cell Quest software were used to analyse the proportions of MDSCs, M1-TAMs and M2-TAMs in tumours and adjacent tissues.

2.11. Western blotting

Total proteins of different samples were extracted with RIPA lysis buffer (Sangon, Shanghai). The protein concentration was basically equal to the bicinchoninic acid (BCA) quantification assay. GAPDH was applied as an internal control. Different proteins were separated by SDS–PAGE and transferred onto PVDF membranes as described previously. The primary antibodies used in this study were VEGF (ab209835), CXCL1 (ab242036), CXCL2 (ab91511) and GM-CSF (ab14024). Immunoreactivity was determined with an

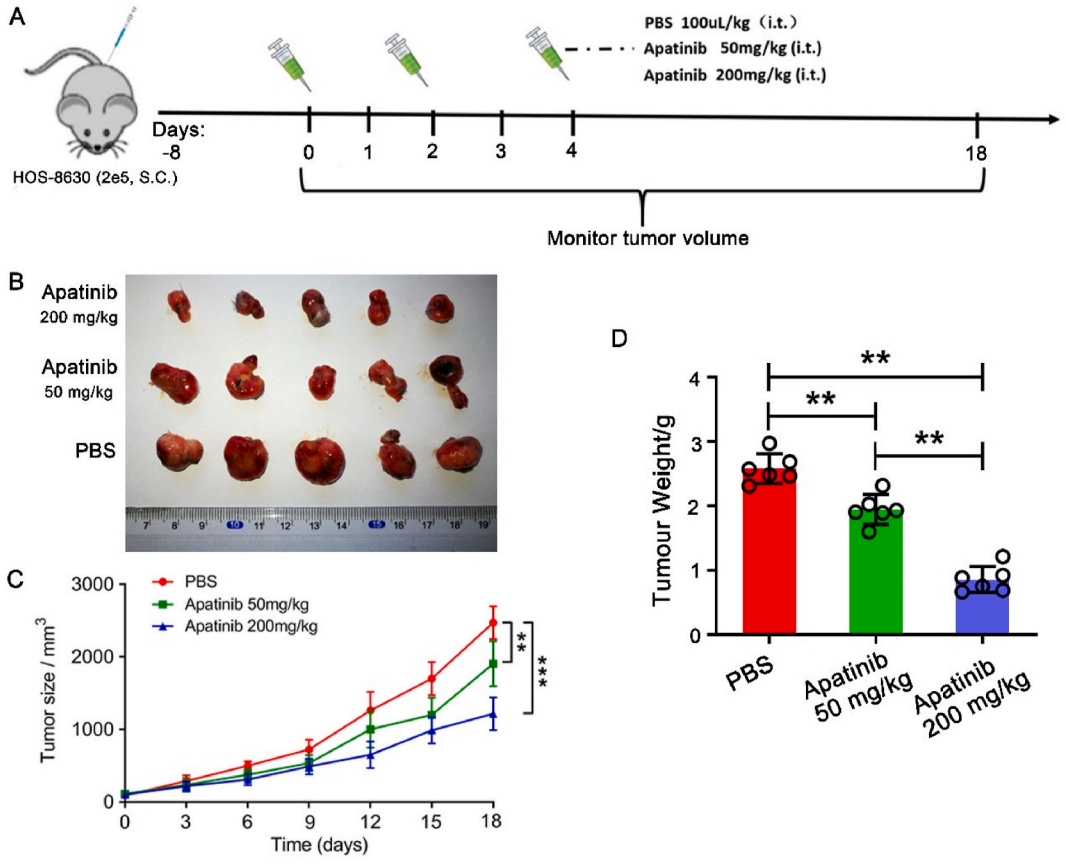

Fig. 1. Tumour growth with apatinib treatment in OS mice. (A) Schematic diagram of the establishment of OS tumour-bearing mice and the administration of apatinib. (B) The morphologies of the tumours after 18 days of the low- and high-dose apatinib treatments compared to the PBS controls. (C) The statistical analysis of the tumour sizes from the two different doses of apatinib treatments every two days, with the PBS group as a control. (D) The statistical analysis of the tumour weight from the two different doses of apatinib treatments with the PBS group as a control. The data were showed as means ± SD, n ≥ 3; $^{**}P < 0.01$, $^{***}P < 0.001$.

enhanced chemiluminescence (ECL) kit (Thermo Fisher, US). The Bio–Rad electrophoresis image analysis system and Quantity One software were applied to form images and analyse the grey value of each target band, and the grey ratios of various target proteins to GAPDH were calculated.

2.12. ELISA

The contents of IL-6, IL-17 and INF-γ in different tumours were detected with an ELISA kit (eBioscience, US) according to the instructions.

2.13. Statistical analysis

All data are presented as the means ± standard deviation (SD) from at least 3 biological repeats. Student's *t-test* and one-way ANOVA were applied to assess the differences in the independent groups. SigmaPlot 12.0 and SPSS 20.1 were used for statistical analysis, and a p value < 0.05 was considered to be statistically significant.

3. Results

3.1. Apatinib suppressed tumour development in a time- and dose-dependent manner

To define the effect of apatinib on tumour development, we administered different doses of apatinib to tumour-bearing mice (Fig. 1A). According to the results from tumour volume observation and statistics, apatinib treatment efficiently suppressed tumour growth (Fig. 1B and C). The tumour volume of the apatinib group was obviously small, and the differences between the apatinib groups and PBS controls became more pronounced over time (Fig. 1C). After 18 days of continuous dosing treatment, the tumours treated with apatinib were significantly smaller than those treated with PBS ($^{**}P < 0.01$, $^{***}P < 0.001$); moreover, those treated with a high dose of apatinib were obviously smaller than those treated with a low dose (Fig. 1B and C). And the results from tumour weight of the three groups were consistent with these findings ($^{**}P < 0.01$) (Fig. 1D).

3.2. Apatinib exhibited multitarget antiangiogenic roles, in which VEGF signalling plays a key role

To identify the molecular targets of apatinib in antitumor effects, we performed protein microarray analysis. According to the results from the protein microarray, a total of 17 pro-/anti-angiogenesis factors, including CCL11, CCL2, CCL3, GM-CSF, IFN-γ, IL-12p70, IL-2, IL-4, IL-6, IL-9, CXCL1, CXCL2, MCPS, SCF, sTNFR1, TIMP 1 and VEGF-A, changed in HOS-8630 cells treated with a

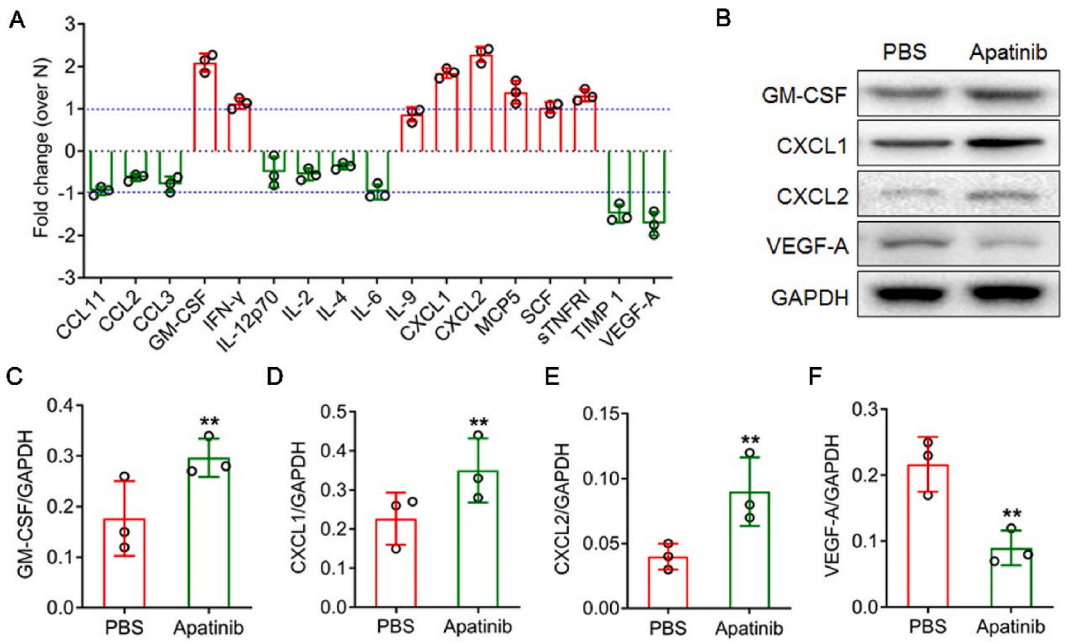

Fig. 2. The protein expression levels of different anti-/pro-angiogenesis cytokines. (A) Protein microarray results showing the differential regulation of the 17 main cytokines after high-dose apatinib treatment. (B) Western blotting results showing the protein expression of VEGF-A, CXCL1, CXCL2 and GM-CSF. (C) Quantitative analysis of the protein expression in B. The data were showed as means ± SD, n ≥ 3; $^{**}P < 0.01$.

high dose of apatinib compared to those treated with PBS (Fig. 2A). Among them, VEGF-A decreased dramatically, and the western blotting results further confirmed this finding (Fig. 2A, B and 2F) (**$P < 0.01$). In addition to VEGF-A, GM-CSF, CXCL1 and CXCL2 showed significantly increased expression with apatinib treatment (Fig. 2A–E) (**$P < 0.01$), which suggested that apatinib was multitargeted in anti-angiogenesis.

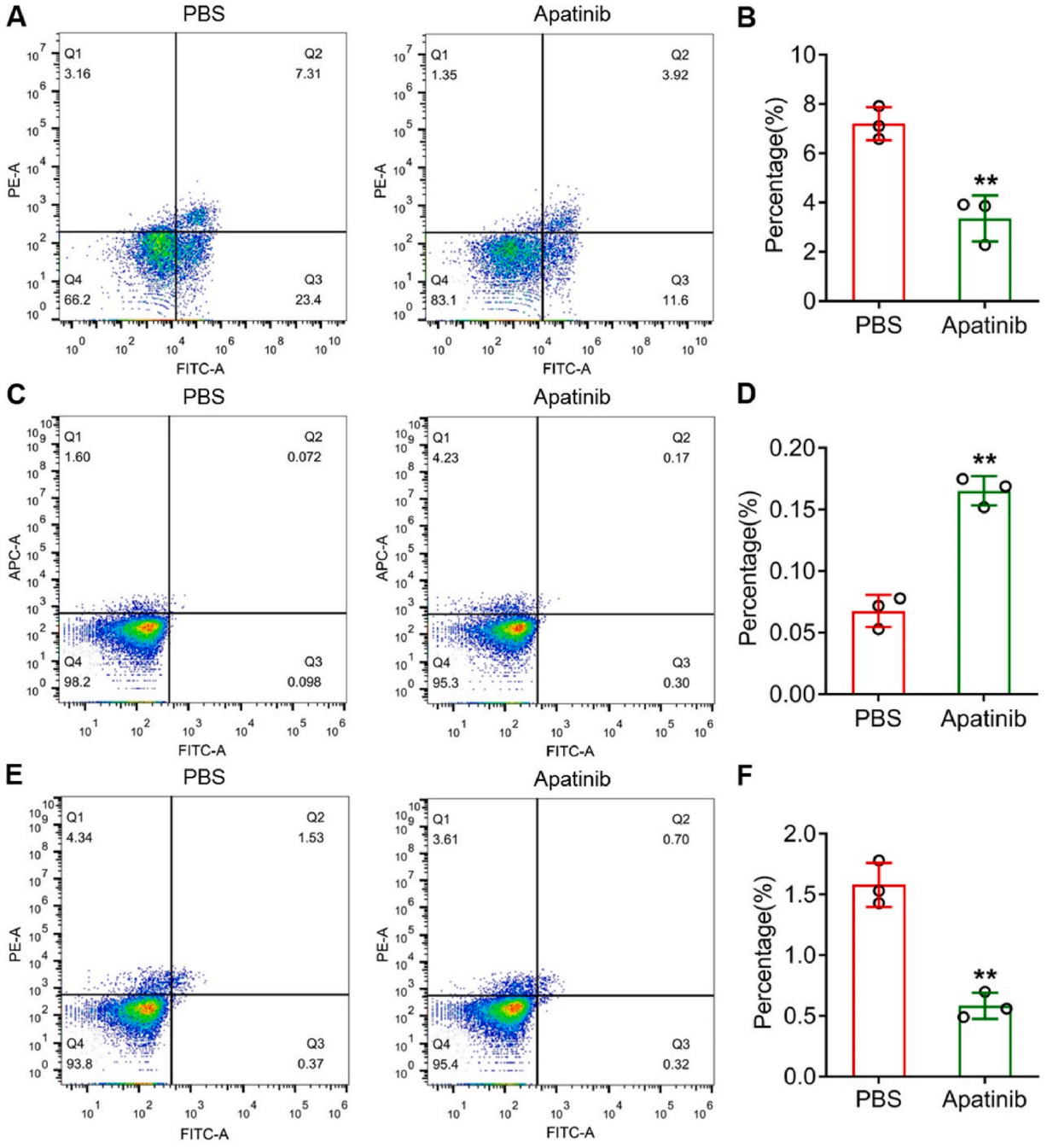

Fig. 3. The ratio of MDSCs, TAM-M1 cells and TAM-M2 cells with apatinib treatment in OS mice. (A) Flow cytometry analysis showed immunosuppressive MDSCs with apatinib treatment compared to PBS treatment. PE labelled anti-Gr-1 antibody, FITC labelled anti-CD11b antibodies. (B) Statistical analysis of the percentage of MADS in A. (C) Flow cytometry analysis showed that TAM-M1 cells were more strongly immunostained with apatinib treatment than with PBS treatment. APC-labelled anti-iNOS antibody, FITC-labelled anti-CD206 antibodies. (D) Statistical analysis of the percentage of TAM-M1 cells in C. (E) Flow cytometry analysis showed the immunosuppressive TAM-M2 cells treated with apatinib compared to those treated with PBS. PE labelled anti-CD68 antibody, FITC labelled anti-CD206 antibodies. (F) Statistical analysis of the percentage of TAM-M2 cells in E. The concentration used in apatinib treatment was 200 mg/kg. The data were showed as means ± SD, n ≥ 3; *$P < 0.05$, **$P < 0.01$.

3.3. Apatinib treatment led to decreases in MDSCs and TAM-M2 cells but an increase in TAM-M1 cells in the mouse tumour microenvironment

As MDSCs and TAMs are important contributors to angiogenesis and the tolerogenic immune state in the OS microenvironment, we analysed the numbers of MDSCs and TAMs in OS mice treated with apatinib. Flow cytometry analysis showed that the ratios of MDSCs and TAM-M2 cells decreased significantly (Fig. 3A, B, 3E and 3F) (*$P < 0.05$, **$P < 0.01$), but that of TAM-M1 cells increased significantly with a high dose of apatinib treatment compared to the PBS controls (Fig. 3C and D) (**$P < 0.01$).

3.4. Apatinib combined with DC-T immunity therapy exhibited a stronger inhibitory effect on OS development

We isolated mouse spleen T lymphocytes and DCs (Suppl. Figs. 1 and 2), prepared HOS-8603 freeze–thaw antigen-specific DCs (Suppl. Fig. 3) and tumour antigen-specific DC-induced T cells (Suppl. Fig. 4), and designed a combination treatment of apatinib with DC-T immunity therapy controlled by PBS administration, a single treatment of apatinib, and DC-T immunity therapy for the established OS mice. After 15 days of different treatments, the tumour sizes of single apatinib treatment or OS antigen-specific DC-T treatment were significantly smaller than those of the PBS controls (**$P < 0.01$) (Fig. 4A and B). In addition, the tumour size with the combination of apatinib and DC-T treatment was much smaller than that of the PBS controls and even significantly smaller than that of the single apatinib or DC-T treatment (**$P < 0.01$) (Fig. 4A and B). The statistical analysis of the tumour weight confirmed the results from tumour size (**$P < 0.01$) (Fig. 4C). MDV detection showed results similar to tumour size observations: single apatinib treatment or OS antigen-specific DC-T treatment significantly reduced the MDV number compared to the PBS controls (*$P < 0.05$), but apatinib and DC-T combination treatment further reduced it to a level that was significantly lower than that of apatinib or DC-T treatment (*$P < 0.05$, **$P < 0.01$) (Fig. 4A and D).

3.5. Apatinib combined with DC-T immunity therapy sharply reduced VEGF expression and changed the release of the cytokines IL-6, IL-17 and IFN-γ in the mouse tumour microenvironment

The western blotting results showed that VEGF protein expression decreased significantly with apatinib or DC-T treatment in OS mice compared to PBS-treated mice (**$P < 0.01$) (Fig. 5A and B). The combination of apatinib and DC-T treatment further reduced the VEGF protein level (**$P < 0.01$), which was significant even compared to apatinib or DC-T treatment alone (**$P < 0.01$) (Fig. 5A and

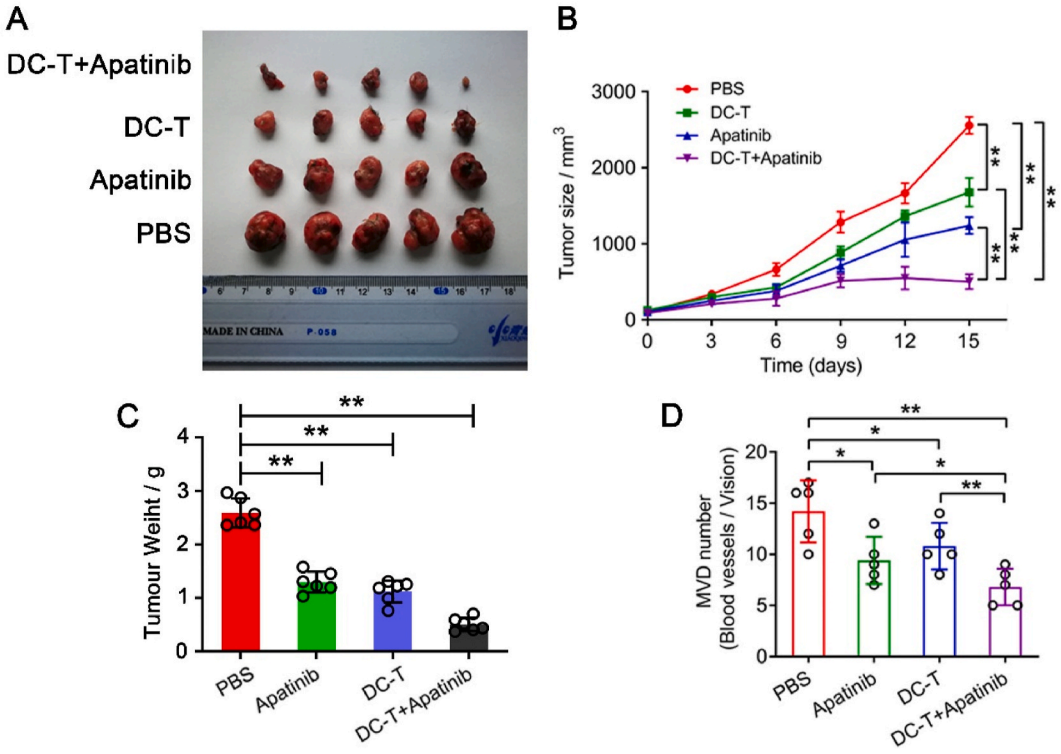

Fig. 4. The effect of apatinib combined with DC-T treatment on OS growth. (A) The morphology of tumours in the DC-T + apatinib, DC-T, and apatinib groups, with PBS treatment as a control. (B) Statistical analysis of the tumour sizes in the four groups. (C) Statistical analysis of the tumour weight in the four groups. (D) MVD number detection in the four groups of mice. The data were showed as means ± SD, n ≥ 3; *$P < 0.05$, **$P < 0.01$.

B). The ELISA results showed that the intracellular release of IL-6 decreased significantly after apatinib or DC-T-cell treatment compared to the PBS controls, and apatinib and DC-T-cell combination treatment reduced it to a low level (**$P < 0.01$), which was even significant compared to the single treatment (*$P < 0.05$, **$P < 0.01$) (Fig. 5C). IL-17 release was decreased after apatinib, DC-T or the combination treatment (*$P < 0.05$, **$P < 0.01$) (Fig. 5C). IL-17 release was lower in the combination treatment group than in the single treatment group (**$P < 0.01$) (Fig. 5C). The release of IFN-γ was the opposite of that of IL-17, and it increased in response to apatinib, DC-T cells or the combination treatment (**$P < 0.01$) (Fig. 5C). The IFN-γ level in the combination-treated group was significantly higher than that in the apatinib-treated or DC-T treatment groups (**$P < 0.01$).

3.6. Apatinib combined with DC-T immunity therapy efficiently suppressed immune-suppressive MDSC proliferation but induced TAM-M1 numbers in the mouse OS microenvironment

The tumour microenvironment is well known to influence therapeutic and clinical outcomes. To evaluate the effect of the combination of apatinib and DC-T treatment on the OS microenvironment, we carried out flow cytometry analysis to detect the number of MDSCs and TAM-M1 cells, which are important components of the tumour microenvironment, in OS mice. The results showed that both apatinib and DC-T-cell treatment significantly reduced the MDSC ratio (**$P < 0.01$) (Fig. 6A and B). However, the combination treatment reduced it to even lower levels (**$P < 0.01$), which was significant even compared to apatinib or DC-T treatment (*$P < 0.05$, **$P < 0.01$) (Fig. 6A and B). The effects on TAM-M1 cells were completely opposite; both apatinib and DC-T treatment enhanced the TAM-M1 ratio significantly (**$P < 0.01$), and the combination treatment increased the TAM-M1 ratio to a higher level (**$P < 0.01$), which was also significant compared to any of the single treatments (**$P < 0.01$) (Fig. 7A and B).

4. Discussion

OS, composed of mesenchymal cells generating immature bone and osteoid, is the most frequent primary malignant bone tumour that mainly affects children and young individuals [1,33]. Approximately one-fourth of OS patients have local invasion and metastases [34]. Current therapeutic management focusing on the combination of surgery and chemotherapy obviously increases long-term survival but remains insufficient, as the cure rate has not improved satisfactorily in the past 3 decades [35]. Efforts to explore better schemes are urgently needed.

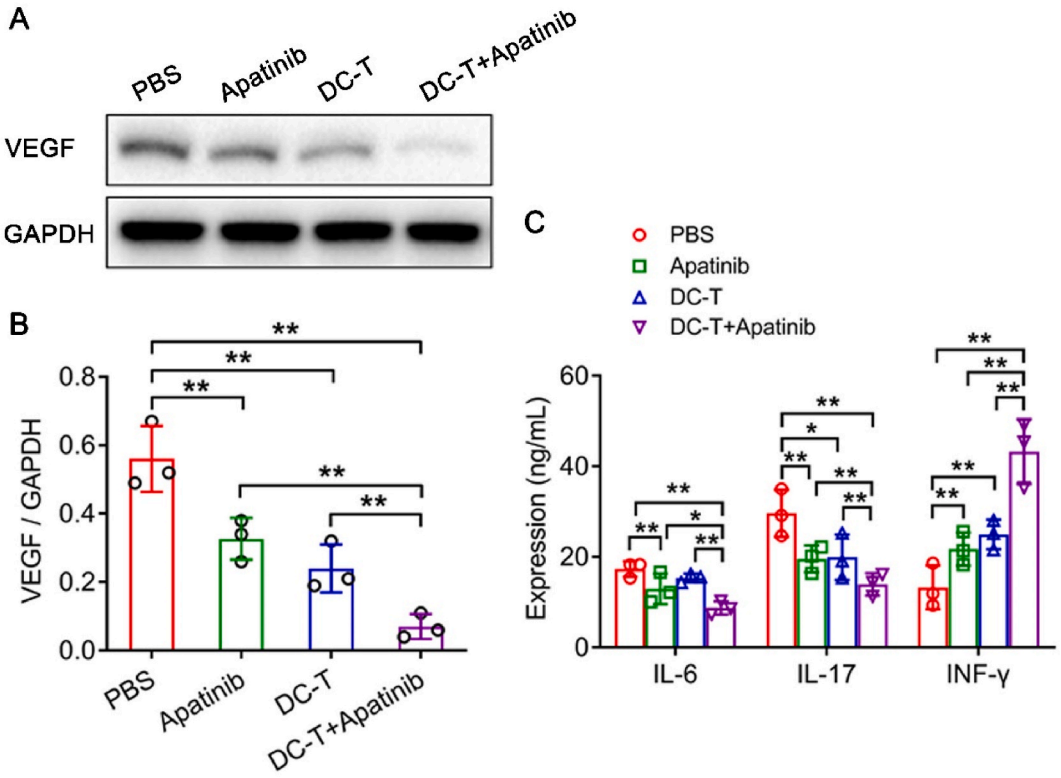

Fig. 5. The expression levels of VEGF, IL-6, IL-17 and INF-γ in apatinib combined with DC-T treatment. (A) Western blotting results showing the protein expression of VEGF normalized to GAPDH in the DC-T + apatinib, DC-T, and apatinib groups, with PBS treatment as a control. (B) Quantitative analysis of VEGF levels in A. (C) ELISA results showing the intracellular release of IL-6, IL-17 and INF-γ in the four groups. The data were showed as means ± SD, n ≥ 3; *$P < 0.05$, **$P < 0.01$.

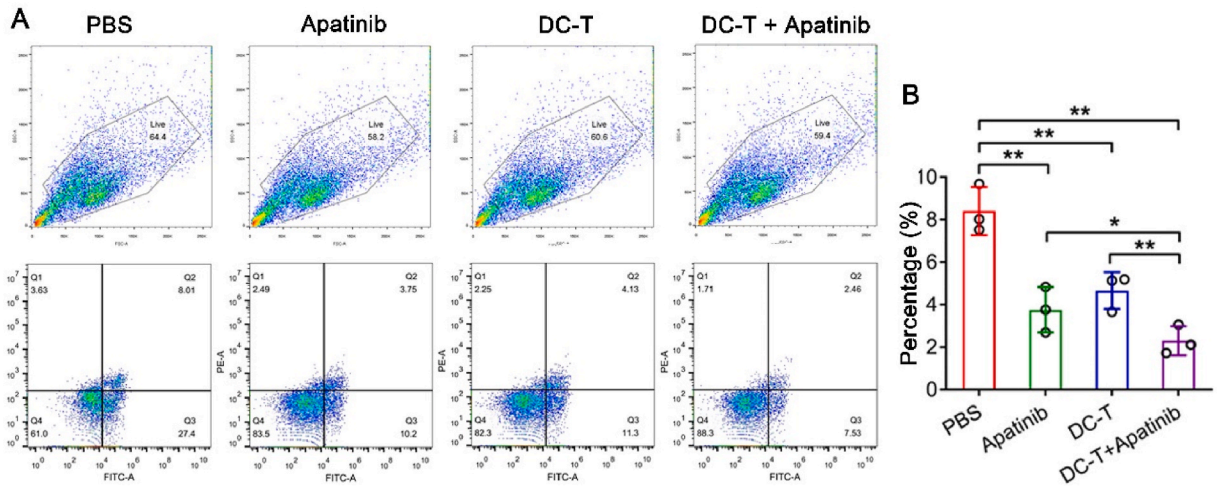

Fig. 6. Ratio of MDSCs to apatinib and DC-T immune cells combined therapy in OS mice. (A) Flow cytometry analysis showing MDSCs treated with apatinib, DC-T cells and apatinib and DC-T cells compared to the PBS control. PE labelled anti-Gr-1 antibody, FITC labelled anti-CD11b antibody. (B) Statistical analysis of the percentage of MADS in A. The concentration used in the apatinib treatment was 200 mg/kg. The data were showed as means ± SD, n ≥ 3; $*P < 0.05$, $**P < 0.01$.

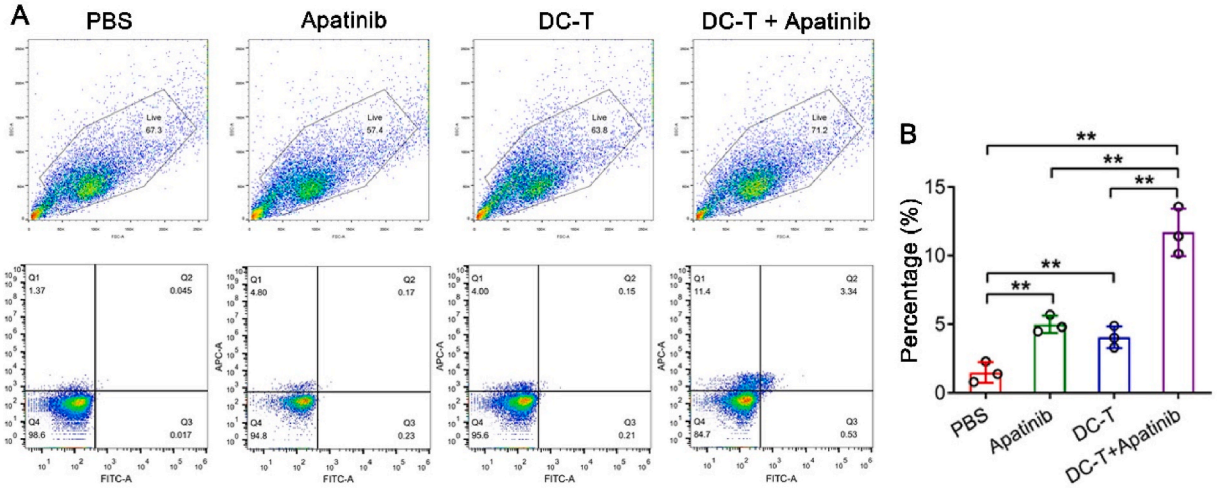

Fig. 7. Ratio of TAM-M1 cells treated with apatinib and DC-T immune cells combined therapy in OS mice. (A) Flow cytometry analysis showing TAM-M1 cells treated with apatinib, DC-T cells and apatinib and DC-T cells compared to the PBS control. APC-labelled anti-iNOS antibody, FITC-labelled anti-CD206 antibody. (B) Statistical analysis of the percentage of TAM-M1 cells in A. The concentration used in apatinib treatment was 200 mg/kg. The data were showed as means ± SD, n ≥ 3; $**P < 0.01$.

The antitumor effect of apatinib in human OS has been well confirmed since the finding that apatinib promotes tumour cell autophagy and apoptosis to inhibit OS growth by blocking VEGFR2/STAT3/BCL-2 signalling [35]. A recent study indicated that apatinib prevents OS cell proliferation and migration [36]. Apatinib has been proven to be an efficient drug for OS patients [37]. Several clinical studies aimed to assess the efficacy of apatinib in advanced osteosarcoma progressing after chemotherapy. In an open label phase II trial, the administration of apatinib in advanced osteosarcoma showed a high objective response rate (ORR, 43.24 %) and the median progression free survival (PFS) and overall survival were 4.50 and 9.87 months, respectively [38]. As antiangiogenic agents might modulate the tumor immunosuppressive microenvironment, the combination therapy of apatinib and immunomodulatory agents was also conducted in osteosarcoma. In a single-arm, phase 2 trial, apatinib plus camrelizumab (anti-PD1 therapy) resulted in an objective response rate of 20.9 % (9/43). They found patients with programmed cell death 1 ligand-1 (PD-L1) tumor proportion score ≥5 % tended to have a longer PFS in comparison to the others [39]. In addition, multi-antigen stimulated cell therapy-I plus camrelizumab and apatinib achieved similar ORR (33.3 %) in patients with advanced osteosarcoma [40]. In this study, both low- and high-dose apatinib treatment significantly reduced the tumour volume, which suggested that apatinib successfully inhibited OS growth. The inhibitory effect of apatinib on tumours was more pronounced with prolonged treatment. Moreover, the high-dose

apatinib application revealed a stronger suppressive effect on tumour growth. These results indicated that the antitumor effect of apatinib was time- and dose-dependent, which was consistent with previous findings [37].

Several studies explored the immunomodulatory role of apatinib in tumour on genomic level. Luo et al. showed that the CellCycle population of malignant gastric epithelium recruits tumor-associated neutrophils (TANs) through the CXCL5/CXCR2 axis to remodel an immunosuppressive tumor microenvironment during anti-PD-1 immunotherapy. However, this phenomenon is compromised by combined apatinib treatment [41]. In a clinical trial exploring the efficacy of camrelizumab plus apatinib in resectable hepatocellular carcinoma (HCC), the researchers found DCs can act as the predictive biomarkers of neoadjuvant therapy as the higher the DCs after neoadjuvant therapy, the less likely patients are to relapse based on TIME analysis [42]. Tumour antigen-specific DC-T-cell immunity therapy has been an emerging field for the clinical treatment of various tumours [43]. Due to the complexity of the immune response, oncolytic immunotherapies targeting DC-T cells have not yet matured in human trials, and the combination of immunotherapy with other therapeutic agents is on track for tumour treatment [44]. In this study, HOS-8603 antigen-specific DC-T treatment inhibited tumour growth similar to apatinib in OS mice, which confirmed previous findings that antigen-presenting DC-induced T immunotherapy inhibited transplanted tumour growth in mice [45]. In addition, the combination of high-dose apatinib and OS antigen-specific DC-T-cell treatment reduced the tumour size to even lower levels than apatinib or DC-T-cell treatment alone, which suggested that the combination of tumour antigen-specific DC-T-cell immunotherapy with antitumor antibodies was promising and an option for OS treatment.

Many kinds of immune cells infiltrate the tumour microenvironment and promote tumour progression and expansion in patients [46,47]. Among them, MDSCs are one of the major components exerting immune suppressive activity, protecting tumours from immune recognition [48,49]. In this study, the ratio of MDSCs was reduced by apatinib or antigen-specific DC-T-cell treatment, while the combination treatment kept it at a lower level. However, the opposite was true for TAM-M1. TAM is another key component in the tumour microenvironment, and the M1 type has been demonstrated to prompt an immune response and suppress tumours [50,51]. Taken together, these results indicated that not only apatinib but also antigen-specific DC-T treatment alleviated the immunosuppressive effect of the OS microenvironment, but their combination therapy improved the immune activity of the tumour microenvironment more efficiently.

In this study, the protein levels of VEGF, IL-6 and IL-17 were decreased, but IFN-γ levels were increased in the apatinib treatment, and the combination therapy was more efficient in changing their expression. In local lung cancer treatment, patients treated with apatinib exhibited decreased IL-6 levels [52]. Recent research suggested that apatinib downregulated IL-17 expression, attenuating tumour proliferation and improving clinical efficacy [53]. The cytokines IL-6, IL-17 and IFN-γ are potent mediators that regulate MDSC and TAM activity [54–57]. Thus, we indicated that the combination of apatinib and OS antigen-specific DC-T therapy strengthened the suppressive effects of apatinib on VEGF, IL-6 and IL-17 expression and the proangiogenic role of apatinib on IFN-γ release in antiangiogenesis, which might be beneficial for improving immune activity in the OS microenvironment and consequently remodelling it to inhibit tumour growth.

5. Conclusion

This study confirmed that antiangiogenic therapy could increase the effectiveness of immunotherapy and provided a promising strategy for OS treatment. Considering the uncertainties in OS patients, human trials are needed in the future to verify the feasibility of the combination of VEGF-TKI drugs with antigen-specific DC-induced T immunotherapy.

Funding

This study was supported by the funds from the National Natural Science Foundation of China (Grant No. 81302342) and the Genertec Guozhong Healthcare (Grant No. GZKJ-KJXX-QTHT-20220016).

Ethical approval

The research was approved by the Medical Ethics Committee of Fudan University Shanghai Cancer Center and Shanghai Medical College, Fudan University (Approval number: FUSCC-IACUC-S20210179).

Consent for publication

All authors have read and agreed to the publishing of this manuscript.

Data availability

Data will be made available on request.

CRediT authorship contribution statement

Tu Hu: Writing – original draft, Resources, Methodology, Formal analysis, Conceptualization. **Wei Sun:** Writing – original draft, Resources, Project administration, Investigation, Formal analysis, Conceptualization. **Yongjia Jin:** Resources, Project administration,

Methodology, Formal analysis, Conceptualization. **Yan Dong:** Resources, Methodology, Data curation. **Wanlin Liu:** Resources, Methodology, Formal analysis, Data curation. **Zhengwang Sun:** Validation, Resources, Methodology, Formal analysis, Data curation. **Yang Xiang:** Writing – review & editing, Project administration, Conceptualization. **Yong Chen:** Writing – review & editing, Project administration, Conceptualization.

Declaration of competing interest

The authors declare the following financial interests/personal relationships which may be considered as potential competing interests:

Not applicable reports was provided by No. No reports a relationship with No that includes:. No has patent No pending to No. All authors declare that they have no conflicts of interest. If there are other authors, they declare that they have no known competing financial interests or personal relationships that could have appeared to influence the work reported in this paper.

Acknowledgments

Not applicable.

Appendix A. Supplementary data

Supplementary data to this article can be found online at https://doi.org/10.1016/j.heliyon.2024.e36016.

References

[1] I. Corre, F. Verrecchia, V. Crenn, F. Redini, V. Trichet, The osteosarcoma microenvironment: a complex but targetable ecosystem, Cells 9 (2020) 976.
[2] M. Kansara, M.W. Teng, M.J. Smyth, D.M. Thomas, Translational biology of osteosarcoma, Nat. Rev. Cancer 14 (2014) 722–735.
[3] D. Cheng, X. Qiu, M. Zhuang, C. Zhu, H. Zou, A. Zhang, Development and validation of nomogram based on miR-203 and clinicopathological characteristics predicting survival after neoadjuvant chemotherapy and surgery for patients with non-metastatic osteosarcoma, Oncotarget 8 (2017) 96935–96944.
[4] Y. Han, X. Zhao, Y. Sun, Y. Sui, J. Liu, Effects of FOSL1 silencing on osteosarcoma cell proliferation, invasion and migration through the ERK/AP-1 signaling pathway, J. Cell. Physiol. 234 (2019) 3598–3612.
[5] W. Wang, J. Yang, Y. Wang, D. Wang, G. Han, J. Jia, et al., Survival and prognostic factors in Chinese patients with osteosarcoma: 13-year experience in 365 patients treated at a single institution, Pathol, Res. Pract. 213 (2017) 119–125.
[6] S. Ferrari, M. Serra, An update on chemotherapy for osteosarcoma, Expet Opin. Pharmacother. 16 (2015) 2727–2736.
[7] W. Yu, Y. Wang, J. Zhu, L. Jin, B. Liu, K. Xia, et al., Autophagy inhibitor enhance ZnPc/BSA nanoparticle induced photodynamic therapy by suppressing PD-L1 expression in osteosarcoma immunotherapy, Biomaterials 192 (2019) 128–139.
[8] A. Bruno, A. Pagani, E. Magnani, T. Rossi, D.M. Noonan, A.R. Cantelmo, et al., Inflammatory angiogenesis and the tumor microenvironment as targets for cancer therapy and prevention, Cancer Treat Res. 159 (2014) 401–426.
[9] M. Paez-Ribes, E. Allen, J. Hudock, T. Takeda, H. Okuyama, F. Vinals, et al., Antiangiogenic therapy elicits malignant progression of tumors to increased local invasion and distant metastasis, Cancer Cell 15 (2009) 220–231.
[10] J. Samples, M. Willis, N. Klauber-Demore, Targeting angiogenesis and the tumor microenvironment, Surg. Oncol. Clin. 22 (2013) 629–639.
[11] S.A. Rosenberg, Overcoming obstacles to the effective immunotherapy of human cancer, Proc. Natl. Acad. Sci. U S A 105 (2008) 12643–12644.
[12] E.A. Vasievich, L. Huang, The suppressive tumor microenvironment: a challenge in cancer immunotherapy, Mol. Pharm. 8 (2011) 635–641.
[13] S.R. Baglio, T. Lagerweij, M. Perez-Lanzon, X.D. Ho, N. Leveille, S.A. Melo, et al., Blocking tumor-educated MSC paracrine activity halts osteosarcoma progression, Clin. Cancer Res. 23 (2017) 3721–3733.
[14] X.D. Ho, P. Phung, Q.L. Van, H.N. Van, E. Reimann, E. Prans, et al., Whole transcriptome analysis identifies differentially regulated networks between osteosarcoma and normal bone samples, Exp. Biol. Med. (Maywood) 242 (2017) 1802–1811.
[15] L. Zhang, S. Yu, S. Hong, X. Xiao, Z. Liao, Y. Li, et al., Comprehensive analysis of BTNL9 as a prognostic biomarker correlated with immune infiltrations in thyroid cancer, BMC Med. Genomics 16 (2023) 234.
[16] K. Cheng, W. Li, H. Wu, C. Li, Mapping knowledge structure and themes trends of cancer-associated fibroblasts: a text-mining study, Front. Mol. Biosci. 10 (2023) 1302016.
[17] X.D. Ho, H.G. Nguyen, L.H. Trinh, E. Reimann, E. Prans, G. Koks, et al., Analysis of the expression of repetitive DNA elements in osteosarcoma, Front. Genet. 8 (2017) 193.
[18] E. Reimann, S. Koks, X.D. Ho, K. Maasalu, A. Martson, Whole exome sequencing of a single osteosarcoma case–integrative analysis with whole transcriptome RNA-seq data, Hum. Genomics 8 (2014) 20.
[19] C. Viallard, B. Larrivee, Tumor angiogenesis and vascular normalization: alternative therapeutic targets, Angiogenesis 20 (2017) 409–426.
[20] D. Hanahan, R.A. Weinberg, Hallmarks of cancer: the next generation, Cell 144 (2011) 646–674.
[21] M. Detmar, Tumor angiogenesis, J. Investig. Dermatol. Symp. Proc. 5 (2000) 20–23.
[22] R.S. Apte, D.S. Chen, N. Ferrara, VEGF in signaling and disease: beyond discovery and development, Cell 176 (2019) 1248–1264.
[23] C.S. Melincovici, A.B. Bosca, S. Susman, M. Marginean, C. Mihu, M. Istrate, et al., Vascular endothelial growth factor (VEGF) - key factor in normal and pathological angiogenesis, Rom. J. Morphol. Embryol. 59 (2018) 455–467.
[24] P. Carmeliet, VEGF as a key mediator of angiogenesis in cancer, Oncology 69 (2005) 4–10.
[25] K. Peng, Y. Bai, Q. Zhu, B. Hu, Y. Xu, Targeting VEGF-neuropilin interactions: a promising antitumor strategy, Drug. Discov. Today 24 (2019) 656–664.
[26] K.S. Siveen, K. Prabhu, R. Krishnankutty, S. Kuttikrishnan, M. Tsakou, F.Q. Alali, et al., Vascular endothelial growth factor (VEGF) signaling in tumour vascularization: potential and challenges, Curr. Vasc, Pharmacol. 15 (2017) 339–351.
[27] R.K. Shrimali, Z. Yu, M.R. Theoret, D. Chinnasamy, N.P. Restifo, S.A. Rosenberg, Antiangiogenic agents can increase lymphocyte infiltration into tumor and enhance the effectiveness of adoptive immunotherapy of cancer, Cancer Res 70 (2010) 6171–6180.
[28] N. Singh, D. Baby, J.P. Rajguru, P.B. Patil, S.S. Thakkannavar, V.B. Pujari, Inflammation and cancer, Ann. Afr. Med. 18 (2019) 121–126.
[29] K. Middleton, J. Jones, Z. Lwin, J.I. Coward, Interleukin-6: an angiogenic target in solid tumours, Crit. Rev. Oncol. Hematol. 89 (2014) 129–139.
[30] Q. Huang, L. Duan, X. Qian, J. Fan, Z. Lv, X. Zhang, et al., IL-17 promotes angiogenic factors IL-6, IL-8, and Vegf production via Stat1 in lung adenocarcinoma, Sci. Rep. 6 (2016) 36551.

[31] J. Zhao, X. Chen, T. Herjan, X. Li, The role of interleukin-17 in tumor development and progression, J. Exp. Med. 217 (2020) e20190297.
[32] V.K. Kommineni, C.N. Nagineni, A. William, B. Detrick, J.J. Hooks, IFN-gamma acts as anti-angiogenic cytokine in the human cornea by regulating the expression of VEGF-A and sVEGF-R1, Biochem. Biophys. Res. Commun. 374 (2008) 479–484.
[33] C. Chen, L. Xie, T. Ren, Y. Huang, J. Xu, W. Guo, Immunotherapy for osteosarcoma: fundamental mechanism, rationale, and recent breakthroughs, Cancer Lett 500 (2021) 1–10.
[34] S. Tsukamoto, C. Errani, A. Angelini, A.F. Mavrogenis, Current treatment considerations for osteosarcoma metastatic at presentation, Orthopedics 43 (2020) e345–e358.
[35] K. Liu, T. Ren, Y. Huang, K. Sun, X. Bao, S. Wang, et al., Apatinib promotes autophagy and apoptosis through VEGFR2/STAT3/BCL-2 signaling in osteosarcoma, Cell Death Dis 8 (2017) e3015.
[36] G. Han, Q. Guo, N. Ma, W. Bi, M. Xu, J. Jia, Apatinib inhibits cell proliferation and migration of osteosarcoma via activating LINC00261/miR-620/PTEN axis, Cell Cycle 20 (2021) 1785–1798.
[37] H. Yao, X. Chen, X. Tan, Efficacy and safety of apatinib in the treatment of osteosarcoma: a single-arm meta-analysis among Chinese patients, BMC Cancer 21 (2021) 449.
[38] L. Xie, J. Xu, X. Sun, X. Tang, T. Yan, R. Yang, et al., Anorexia, hypertension, pneumothorax, and hypothyroidism: potential signs of improved clinical outcome following apatinib in advanced osteosarcoma, Cancer Manag. Res. 12 (2020) 91–102.
[39] L. Xie, J. Xu, X. Sun, W. Guo, J. Gu, K. Liu, et al., Apatinib plus camrelizumab (anti-PD1 therapy, SHR-1210) for advanced osteosarcoma (APFAO) progressing after chemotherapy: a single-arm, open-label, phase 2 trial, J. Immunother. Cancer 8 (2020) e000798.
[40] Y. Zhou, M. Li, B. Zhang, C. Yang, Y. Wang, S. Zheng, et al., A pilot study of multi-antigen stimulated cell therapy-I plus camrelizumab and apatinib in patients with advanced bone and soft-tissue sarcomas, BMC Med. 21 (2023) 470.
[41] Q. Luo, Z. Dong, W. Xie, X. Fu, L. Lin, Q. Zeng, et al., Apatinib remodels the immunosuppressive tumor ecosystem of gastric cancer enhancing anti-PD-1 immunotherapy, Cell Rep. 42 (2023) 112437.
[42] Y. Xia, W. Tang, X. Qian, X. Li, F. Cheng, K. Wang, et al., Efficacy and safety of camrelizumab plus apatinib during the perioperative period in resectable hepatocellular carcinoma: a single-arm, open label, phase II clinical trial, J. Immunother. Cancer 10 (2022) e004656.
[43] P. Wehr, H. Purvis, S.C. Law, R. Thomas, Dendritic cells, T cells and their interaction in rheumatoid arthritis, Clin. Exp. Immunol. 196 (2019) 12–27.
[44] I. Lurje, L. Hammerich, F. Tacke, Dendritic cell and T cell crosstalk in liver fibrogenesis and hepatocarcinogenesis: implications for prevention and therapy of liver cancer, Int. J. Mol. Sci. 21 (2020) 7378.
[45] S.K. Nair, D. Snyder, B.T. Rouse, E. Gilboa, Regression of tumors in mice vaccinated with professional antigen-presenting cells pulsed with tumor extracts, Int. J. Cancer 70 (1997) 706–715.
[46] Y. Oya, Y. Hayakawa, K. Koike, Tumor microenvironment in gastric cancers, Cancer Sci. 111 (2020) 2696–2707.
[47] X. Tian, H. Shen, Z. Li, T. Wang, S. Wang, Tumor-derived exosomes, myeloid-derived suppressor cells, and tumor microenvironment, J. Hematol. Oncol. 12 (2019) 84.
[48] R.J. Tesi, MDSC; the most important cell you have never heard of, Trends Pharmacol. Sci. 40 (2019) 4–7.
[49] V. Kumar, S. Patel, E. Tcyganov, D.I. Gabrilovich, Gabrilovich, the nature of myeloid-derived suppressor cells in the tumor microenvironment, Trends Immunol. 37 (2016) 208–220.
[50] K. Zhou, T. Cheng, J. Zhan, X. Peng, Y. Zhang, J. Wen, et al., Targeting tumor-associated macrophages in the tumor microenvironment, Oncol. Lett. 20 (2020) 234.
[51] H. Li, M. Somiya, S. Kuroda, Enhancing antibody-dependent cellular phagocytosis by Re-education of tumor-associated macrophages with resiquimod-encapsulated liposomes, Biomaterials 268 (2021) 120601.
[52] Y. Feng, B. Yang, X. Li, Clinical analysis of 125I seed implantation combined with apatinib in the treatment of locally advanced lung cancer: a case series, J. Pak, Med. Assoc. 71 (2021) 1025–1027.
[53] R. Chen, Q.T. Chen, Y.H. Dong, Clinical efficacy of apatinib in treating metastatic gastric cancer and its effect on IL-17, Oncol. Lett. 17 (2019) 5447–5452.
[54] R. Weber, C. Groth, S. Lasser, I. Arkhypov, V. Petrova, P. Altevogt, et al., IL-6 as a major regulator of MDSC activity and possible target for cancer immunotherapy, Cell. Immunol. 359 (2021) 104254.
[55] M. Ma, W. Huang, D. Kong, IL-17 inhibits the accumulation of myeloid-derived suppressor cells in breast cancer via activating STAT3, Int. Immunopharmacol. 59 (2018) 148–156.
[56] B. Cai, Y. Liu, Y. Chong, H. Zhang, A. Matsunaga, X. Fang, et al., IRAK1-regulated IFN-gamma signaling induces MDSC to facilitate immune evasion in FGFR1-driven hematological malignancies, Mol. Cancer 20 (2021) 165.
[57] J. Shen, X. Sun, B. Pan, S. Cao, J. Cao, D. Che, et al., IL-17 induces macrophages to M2-like phenotype via NF-kappaB, Cancer Manag. Res. 10 (2018) 4217–4228.